

# Contributions of Conformational Flexibility to High-Affinity Zinc Binding in the Solute Binding Protein AztC

Fred A. Serrano and Erik T. Yukl\*

Cite This: *ACS Omega* 2022, 7, 3768–3774

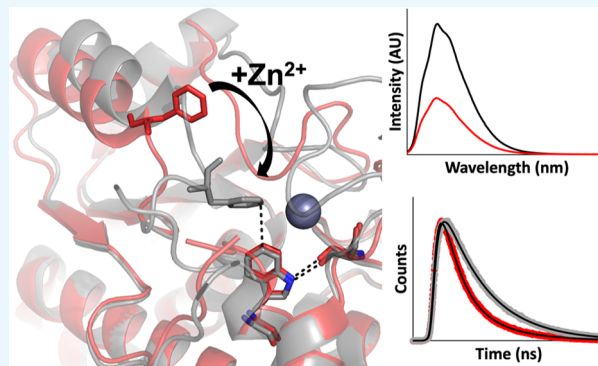
Read Online

ACCESS |

Metrics &amp; More

Article Recommendations

**ABSTRACT:** Bacteria rely on ATP binding cassette (ABC) transporters for the import of various nutrients. Bacterial ABC importers utilize an extracellular solute binding protein (SBP) to bind the substrate with high affinity and specificity and deliver it to the membrane permease for transport. The essential metals iron, manganese, and zinc are bound and transported by the cluster A–I SBPs. Crystal structures exist for the metal-bound and metal-free forms of several cluster A–I SBPs that show relatively subtle conformational changes that accompany metal binding. Recent solution studies and molecular dynamics simulations indicate a more complex conformational landscape for the cluster A–I SBPs, suggesting that changes in protein dynamics upon metal binding may have an important role in recognition by the membrane permease and effective transport. Here, we investigate conformational states and dynamics in the cluster A–I SBP AztC from *Paracoccus denitrificans*, characterizing its unusual intrinsic fluorescence behavior and thermodynamics of zinc binding. These data suggest a dynamic equilibrium of at least two conformational states in the apo form and compensatory changes in the holo that provide for a significant entropic contribution to zinc binding. Correlation with available crystal structures suggests that the formation of a Trp–Phe  $\pi$ -stacking interaction in the metal-bound form may mediate the observed changes in fluorescence. The conformational dynamics identified here for AztC are likely applicable to other cluster A–I SBPs with relevance to their exploitation as potential antibiotic drug targets.



## INTRODUCTION

ATP binding cassette (ABC) transporters mediate the active transport of a wide variety of molecules and ions in all kingdoms of life.<sup>1</sup> Substrates cross the membrane through two transmembrane domains or subunits, while two nucleotide binding domains or subunits power the process through ATP hydrolysis. In bacteria, ABC transporters can function to import essential nutrients. In this case, a periplasmic (Gram-negative) or outer membrane-tethered (Gram-positive) solute binding protein (SBP) is required<sup>2,3</sup> to bind the substrate with high affinity and specificity and deliver it to the permease for import into the cytoplasm.<sup>4</sup>

Although they transport a vast array of diverse substrates, SBP structures are remarkably similar with the substrate binding site in a cleft between two structurally related  $\alpha/\beta$  domains. The structure of the interdomain linker allows the SBPs to be classified into seven clusters (A–G)<sup>5</sup> with further subdivisions based on substrate specificity. Binding of the cognate substrate is generally thought to mediate a conformational switch between open and closed forms that is essential for recognition by the membrane permease and subsequent substrate transport.<sup>2,6</sup> In the case of the well-studied cluster B–I proteins, which include maltose binding protein, these

changes are quite dramatic and have been described as a “Venus fly trap”.<sup>7</sup> However, this does not appear to be true of all SBPs.

The cluster A–I SBPs mediate the transport of zinc, manganese, or iron, binding the metal between domains linked by a long  $\alpha$  helix (Figure 1). Numerous crystal structures of these proteins have been solved, including some in both holo and apo states. Generally, these structures indicate relatively modest structural changes upon metal binding that primarily involve motions of the C-terminal domain (CTD), specifically a loop between  $\beta 6$ – $\alpha 7$ , helix  $\alpha 7$ , and helix  $\alpha 8$ .<sup>8–12</sup> Reorientations of loops in the N-terminal domain (NTD), specifically in  $\beta 2$ – $\alpha 2$  and  $\beta 3$ – $\alpha 3$  loops, have also been noted in some cases.<sup>10–12</sup> Where reported, *B*-factors in these regions also tend to be higher than average, whereas regions distal to

Received: November 23, 2021

Accepted: January 10, 2022

Published: January 20, 2022



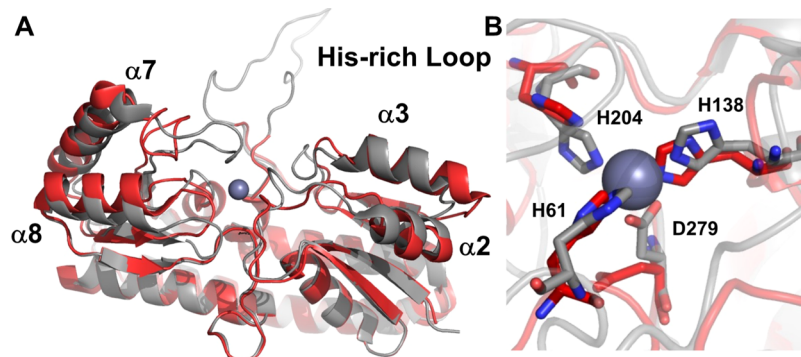


**Figure 1.** Conformational changes between apo (red, PDB ID: 5W56) and zinc-bound (gray, PDB ID: 5W57) *P. denitrificans* AztC.<sup>10</sup> (A) Whole proteins shown as cartoons illustrating conformational changes to the indicated helices and associated loops. (B) Zinc binding site.

the metal binding site appear relatively rigid. However, crystallographic evidence of some cluster A–I SBPs indicates virtually no conformational changes on metal binding<sup>13</sup> or even a slightly more closed conformation in the apo state.<sup>14</sup> Further, while *B*-factor analysis can be informative on regions of relative flexibility, crystallography tends to isolate a single structure from what may be a dynamic equilibrium, particularly where there are small energy differences between conformations. Thus, a two-state model where metal binding is tightly coupled to an open to closed conformational switch may be overly simplistic for many cluster A–I SBPs. Further, dynamic interconversion between conformations may have an important role in substrate specificity, mediating interactions with the permease and subsequent metal transport. As has been extensively reviewed,<sup>15</sup> transition-metal import through ABC transporters is critical for bacterial virulence. The effective exploitation of these systems as antimicrobial drug targets will require a thorough description of the SBP conformational landscape and dynamics.

Recent reports have applied an array of solution techniques to interrogate the dynamics of cluster A–I SBPs. Electron paramagnetic resonance (EPR) and molecular dynamics (MD) simulations<sup>9,16</sup> on the manganese SBP PsaA and MD simulations of the zinc SBP Lmb<sup>17</sup> suggest that the conformational switch between open and closed states is primarily mediated by motions of CTD regions. Single-molecule fluorescence resonance energy transfer (FRET) microscopy studies of PsaA<sup>18</sup> and the zinc SBP AdcA<sup>19</sup> indicate a closer approach of CTD and NTD in the holo form consistent with an open to closed transition upon metal binding. However, these studies revealed distinct mechanisms of metal binding for these proteins despite a high degree of sequence similarity (51% identity). Metal binding to PsaA is accompanied by partial unwinding of the linker helix and a relatively large movement of the CTD to generate the closed form.<sup>9</sup> In contrast, AdcA has a stable linker helix, and only minor domain motions are observed during metal binding. Rather, a dynamic NTD loop  $\beta 2$ – $\alpha 2$  is stabilized by zinc binding in a “trap-door” mechanism of zinc binding.<sup>19</sup> These differences have important implications in metal binding specificity and interactions with membrane permeases and highlight the diversity of conformational landscapes accessible to even close homologues in the cluster A–I SBPs.

Crystal structures of the SBP AztC from *Paracoccus denitrificans* demonstrate changes at both NTD and CTD regions mentioned above (Figure 1), making it a good example of the conformational changes available to the cluster A–I

SBPs. In order to interrogate the conformational changes and dynamics accompanying metal binding for this protein in solution, we leverage its unusual Trp fluorescence properties.<sup>20</sup> The wavelength, intensity, and lifetime of Trp fluorescence are very sensitive to its microenvironment, making it an excellent label-free probe for binding events and/or conformational changes. Fluorescence lifetime is particularly powerful due to its high temporal resolution compared with single-molecule FRET (the ns range compared to the ms range), enabling simultaneous detection of rapidly interconverting conformations and rare events. We also investigate the thermodynamics of zinc binding by isothermal titration calorimetry (ITC). Where possible, we have correlated solution and structural data to present a cohesive picture of conformational changes and dynamics for AztC, validating this model with a mutant lacking critical zinc binding residues His 138 and His 204 (Figure 1B) from the NTD and CTD, respectively. Rapid zinc dissociation from the H138/204A AztC mutant has been previously characterized,<sup>21</sup> and the mutation is predicted to perturb the open–closed conformational equilibrium. The results illustrate that conformational flexibility and entropic contributions are important for high-affinity zinc binding and likely for permease recognition and metal transport.

## EXPERIMENTAL PROCEDURES

**Expression and Purification of Proteins.** WT<sup>22</sup> and H138/204A<sup>21</sup> *P. denitrificans* AztC (Uniprot ID: A1B2F3) were produced as previously described. Briefly, the periplasmic fraction was prepared using an osmotic shock protocol adapted from Wang et al.<sup>23</sup> Proteins were initially purified at pH 8.0 by anion-exchange chromatography using a HiTrap Q HP column (Cytiva) on a gradient of increasing NaCl. Fractions containing AztC were combined and concentrated to <1 mL and further purified using a HiPrep Sephacryl S-200 HR size exclusion column (SEC) (Cytiva) equilibrated with 50 mM Tris pH 8.0, 150 mM NaCl. After final purification by SEC, proteins were highly pure as judged by sodium dodecyl sulfate-polyacrylamide gel electrophoresis. AztC concentrations were determined using an extinction coefficient at 280 nm of 19,691 M<sup>-1</sup> cm<sup>-1</sup>, calculated as previously described.<sup>24</sup>

**Generation of Apo-Proteins and Metal Quantitation.** Apo proteins were generated by dialysis at 4 °C against two changes of 50 mM sodium acetate buffer pH 4.5, 50 mM ethylenediaminetetraacetate, and 150 mM NaCl. This was followed by dialysis against two changes of 50 mM Tris buffer pH 8.0, 150 mM NaCl, and 3.4 g/L Chelex resin (Bio-Rad). Complete zinc removal was confirmed by inductively coupled

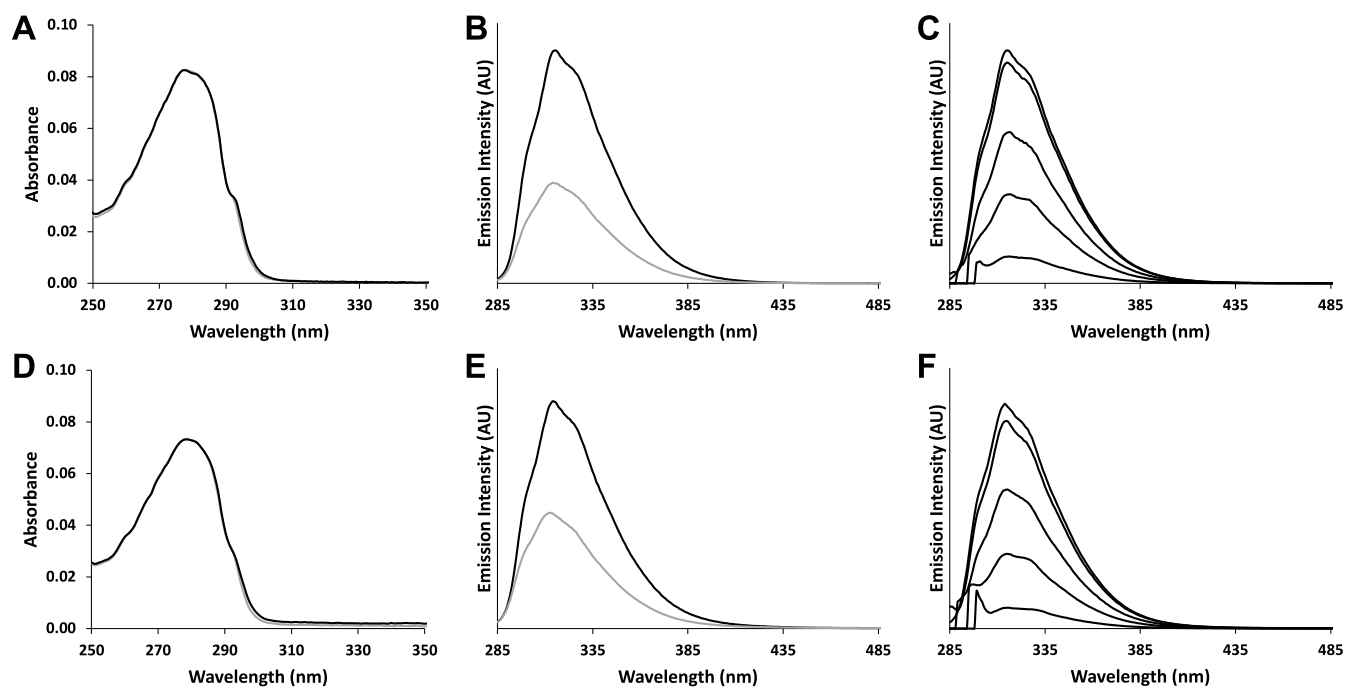


**Figure 2.** Absorption and fluorescence emission spectra for WT AztC (A–C) and H138/204A AztC (D–F). (A,D) absorption spectra for apo (gray) and holo (black) proteins. They overlap so closely as to make it difficult to see that both are presented. (B,E) Fluorescence emission spectra ( $\lambda_{\text{exc}} = 278$  nm) for apo (gray) and holo (black) proteins. Fluorescence spectra parameters are given in Table 1. (C,F) Fluorescence emission for holo proteins at different excitation wavelengths ( $\lambda_{\text{exc}} = 278, 285, 290, 295,$  and  $300$  nm).

plasma-optical emission spectrometry (ICP-OES). Briefly, protein samples at a concentration of 10–20  $\mu\text{M}$  were digested in 4 M  $\text{HNO}_3$  overnight at 70  $^\circ\text{C}$  and diluted 2.5-fold with Milli-Q water prior to metal analysis. Buffer blanks were generated identically using an equal volume of the buffer relative to the protein solution. Metal content was quantified using a PerkinElmer 2100 DV ICP-OES, calibrated with a multielement standard (Alpha Aesar) at a wavelength of 213.857 nm for zinc.

**Determination of Relative Quantum Yields.** Apo proteins were exchanged into metal-free 5 mM sodium phosphate pH 7.2 using Zeba desalting columns (Pierce), and a stock tryptophan solution was made up to  $\sim 10$  mM in the same buffer and centrifuged prior to use. Protein or tryptophan was added to 1.5 mL of phosphate buffer in a stirred quartz cuvette to an  $\text{OD}_{280}$  of approximately 0.02. Absorption spectra between 200 and 500 nm and fluorescence emission spectra ( $\lambda_{\text{exc}} = 278$  nm) from 285 to 500 nm were collected for apo protein samples. To generate holo samples,  $\text{ZnCl}_2$  was then added to approximately 10-fold molar excess. Protein or tryptophan was then added to generate a solution of  $\text{OD}_{280} \sim 0.04, 0.06,$  and  $0.08,$  and the scanning process was repeated after each addition. Holo proteins were maintained in a 10-fold excess of zinc. Quantum yields were determined by plotting absorbance at 278 nm versus the integrated area under the fluorescence emission curve. The slope of the line representing the quantum yield was normalized assuming a tryptophan quantum yield of 0.13.<sup>25</sup> Values are reported from at least three independent experiments.

**Fluorescence Lifetime.** Lifetime data were collected at the end of quantum yield experiments from samples at  $\text{OD}_{280} \sim 0.08$  diluted 2-fold in metal-free phosphate buffer. A solution of 0.01% w/v silicon(IV) oxide in water was used as a scattering prompt. Data were collected using a Horiba

DeltaPro time-correlated single-photon counting system equipped with a DeltaDiode pulsed laser at 281 nm (DD-280, Horiba), neutral density excitation filters, and a 290 nm long-pass emission filter (Thorlabs). Data were collected to 10,000 counts and fitted in DAS6 software.

**Isothermal Titration Calorimetry.** ITC measurements were carried out on a Nano LV-ITC titration calorimeter (TA instruments, Inc.). Apo AztC was exchanged into degassed metal-free 20 mM *N*-(2-hydroxyethyl)piperazine-*N'*-ethanesulfonic acid pH 7.2, 200 mM NaCl using Zeba spin desalting columns and diluted to a final concentration of 50  $\mu\text{M}$  in a volume of 300  $\mu\text{L}$  in this buffer. This was titrated with 2  $\mu\text{L}$  injections of 1.0 mM  $\text{ZnCl}_2$  in the same buffer at 25  $^\circ\text{C}$  and a stir speed of 300 rpm. A blank measurement to determine heats of dilution was conducted in the absence of protein. The blank was subtracted from the WT data, and integrated heat data were directly analyzed using an independent binding model in the NanoAnalyze software (TA Instruments).

## RESULTS

**Fluorescence Quantum Yield and Lifetime.** We had previously shown a roughly two-fold increase in intrinsic protein fluorescence in AztC upon zinc binding.<sup>10</sup> This behavior had not been reported for any other cluster A–I SBP to our knowledge. Further, fluorescence is highly sensitive to the environment of the fluorophore, suggesting that this may be a useful probe of conformational dynamics in this protein. Thus, a more thorough investigation of the spectroscopic properties of AztC was warranted (Figure 2). We also investigated the H138/204A mutant of AztC, predicting that conformational equilibrium between open and closed forms would be perturbed.

The absorption spectra between WT and mutant AztC were very similar and unaffected by the addition of zinc. As

**Table 1. Fluorescence Properties of Zinc Solute Binding Proteins**

sample	$\lambda_{\text{Max,Em}}$ (nm)	quantum yield	$\tau_1$ (ns)	$\tau_2$ (ns)	ratio of pre-exponentials ( $A_1/A_2$ )
Apo <i>Pd</i> AztC	314	$0.071 \pm 0.007$	$3.46 \pm 0.19$	$1.41 \pm 0.05$	$0.85 \pm 0.30$
Holo <i>Pd</i> AztC	315	$0.154 \pm 0.007$	$3.57 \pm 0.22$		
Apo H138/204A <i>Pd</i> AztC	314	$0.066 \pm 0.008$	$3.08 \pm 0.25$	$1.17 \pm 0.03$	$0.65 \pm 0.28$
Holo H138/204A <i>Pd</i> AztC	314	$0.119 \pm 0.013$	$3.39 \pm 0.04$	$1.72 \pm 0.05$	$5.7 \pm 0.9$

predicted, both WT and H138/204A AztC exhibited significant increases in fluorescence emission intensity upon zinc binding, but the band shapes remained constant and were largely independent of excitation wavelength. The fluorescence quantum yields were determined relative to the reported quantum yield of tryptophan in water of 0.13<sup>25</sup> (Table 1) and demonstrate a significant reduction in quantum yield in H138/204A relative to WT in the holo form but not in the apo form.

We also determined the excited-state lifetimes of each protein using time-resolved fluorescence (Figure 3 and Table

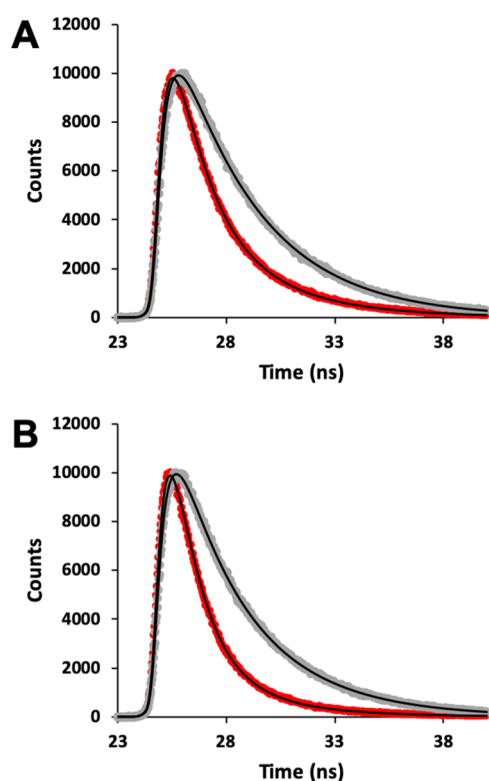


**Figure 3.** Fluorescence decay data for apo (red) and holo (gray) WT AztC (A) and H138/204A AztC (B).  $\lambda_{\text{Exc}} = 280$  nm. Data were fitted (black lines) with parameters listed in Table 1.

1). For WT AztC, two exponentials at comparable amplitudes were required to obtain satisfactory fits of the decay data, while only the longer-lived species ( $\tau_1$ ) was evident for the holo protein. The H138/204A mutant data were similar, except that the overall lifetime in the apo form was reduced and the short-lived species persisted in the holo form, albeit at a reduced relative amplitude.

**Isothermal Titration Calorimetry.** To determine the thermodynamic contributions to zinc binding in AztC, we performed ITC (Figure 4 and Table 2). The data indicate a single zinc binding site with a dissociation constant of 51 nM. This is significantly higher than the  $K_d$  estimated by the MF-2 assay of 0.3 nM,<sup>22</sup> but there is also a large error associated with

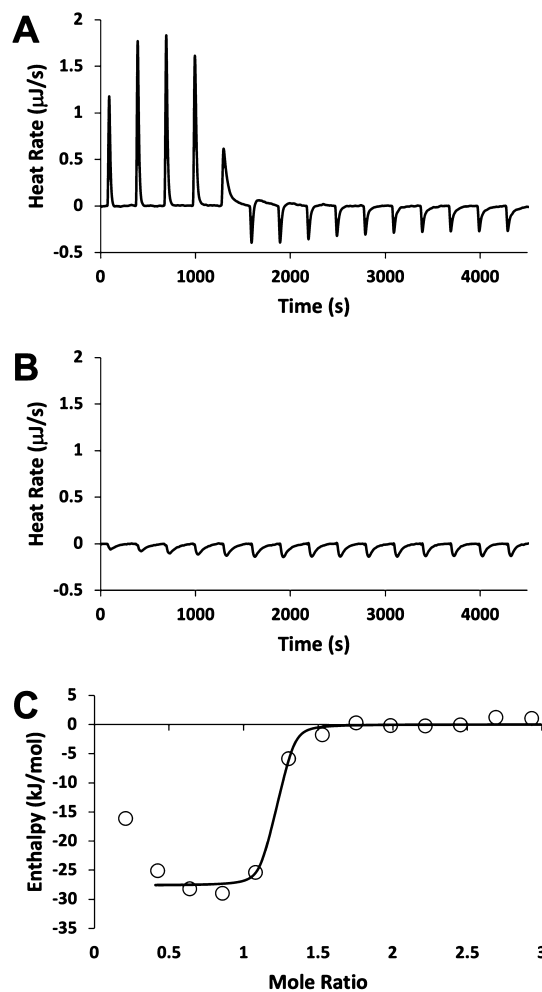


**Figure 4.** Zinc binding to WT AztC by ITC. ITC isotherms and integrated heats of titration are shown for 50  $\mu\text{M}$  WT AztC titrated with 1 mM  $\text{ZnCl}_2$  (A,C). The isotherm for the buffer blank is shown in (B). Solid lines represent fits to the data resulting in binding parameters listed in Table 2.

this value because of the intrinsic limitations of ITC for measuring extremely high-affinity binding events. Binding is exothermic and includes a considerable positive entropic component, which is likely even larger than indicated given the underestimation of binding affinity by this method.

## DISCUSSION

**AztC Fluorescence.** The intrinsic fluorescence behavior of *Pd* AztC is extremely unusual. At 315 nm, the emission maximum of *Pd* AztC is among the most blue-shifted yet determined,<sup>26</sup> and the more than 2-fold increase in quantum yield upon zinc binding is unusually large. The increase in quantum yield is accompanied by the loss of a more rapidly decaying excited state ( $\tau_2$ ), resulting in an overall increase in excited-state lifetime. This behavior is similar to what is

Table 2. WT AztC Zinc Binding Parameters as Determined by ITC<sup>a</sup>

protein	site	<i>n</i>	$\Delta H$ (kJ/mol)	$k_d$ (M)	$\Delta S$ (J/mol·K)
WT AztC	1	1.11 ± 0.03	-27.6 ± 1.5	$5.1 \times 10^{-8} \pm 8.3 \times 10^{-8}$	47.0

<sup>a</sup>Uncertainties are derived for the fit at the 95% confidence interval.

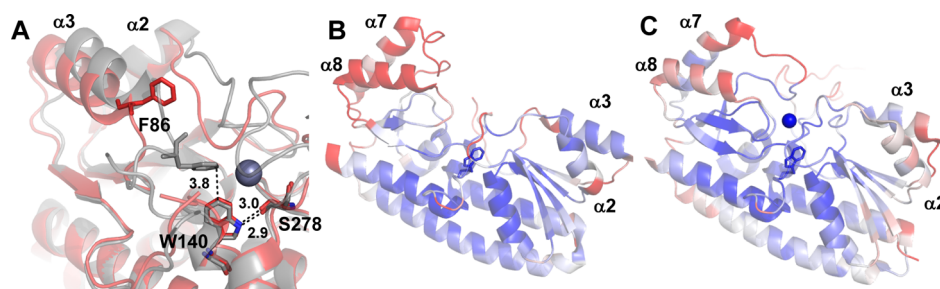


**Figure 5.** Changes in Trp interactions and *B*-factors in apo and holo AztC. (A) Comparison of interactions around Trp 140 in apo (red) and holo (gray) *Pd* AztC. Dotted lines represent molecular interactions with distances given in Å. (B) Apo and (C) holo *Pd* AztC are colored according to *B*-factors, with white indicating the average main chain atomic *B*-factor, blue indicating the average minus the standard deviation, and red indicating the average plus the standard deviation.

observed in the blue copper protein azurin.<sup>27–30</sup> However, the changes in azurin fluorescence upon Cu<sup>+</sup> or Cu<sup>2+</sup> binding are opposite in direction. That is, copper binding quenches azurin fluorescence and results in the appearance of a short-lived excited state in addition to the single long-lived state in apo azurin. The dual exponential decay kinetics for holo azurin have been explained by the existence of two protein conformers at the copper binding site with distinct interactions with a nearby Trp,<sup>27,28</sup> although this interpretation has been challenged.<sup>29</sup> Nevertheless, extending this idea to AztC would indicate two conformations in the apo state that converge to a single conformation upon zinc binding. If this is correct, the open conformation is present only in the apo form and is responsible for the rapidly decaying excited state. The relative amplitudes of each state would indicate that the apo form is primarily in the open conformation, but with a significant fraction in the closed conformation. This is in contrast to what is observed by single-molecule FRET studies of apo PsaA, where a closed conformation was never observed. This may be due to mechanistic differences between these proteins or the lower temporal resolution of this technique, which nevertheless did identify rare closing events in amino acid and peptide SBPs.<sup>18</sup> To our knowledge, this is the first report of a closed apo state for a cluster A–I SBP in solution. However, the crystal structure of the close AztC homologue TroA from *Treponema pallidum* reveals a closed conformation.<sup>14</sup> This is consistent with the idea of a dynamic equilibrium between open and closed states in the apo form where subtle crystal packing interactions can favor one or the other. Further, the persistence of the rapidly decaying conformer in holo H138/204A AztC is consistent with a small population of an open state in the holo form of this mutant, which results in the dramatic increase in zinc off-rate relative to WT.<sup>21</sup>

Because the absorption spectra and fluorescence band shapes are virtually identical, we can assume that the rates of fluorescence decay ( $k_f$ ) for the open and closed forms are essentially equivalent at  $k_f = 0.043 \text{ ns}^{-1}$ .<sup>27</sup> Knowing the quantum yields, we can calculate the rates of nonradiative decay ( $k_{nr}$ ) for closed and open conformations as  $k_{nr1} = 0.24 \text{ ns}^{-1}$  and  $k_{nr2} = 0.67 \text{ ns}^{-1}$ , respectively, indicating that an additional quenching process is operative in the open conformation. Solvent quenching is a possibility, yet Trp 140

appears to be completely shielded from the solvent in both apo and holo structures with essentially negligible solvent accessible surface areas of 0.51 and 1.65 Å<sup>2</sup>, respectively. Similarly, hydrogen bonding between the indole nitrogen and backbone oxygen of Ser 278 is preserved in both structures (Figure 5A). However, close inspection of the Trp 140 environment reveals one significant difference in holo and apo forms that is mediated by changes in the NTD. Partial unwinding and shifting of helix  $\alpha 3$  along with reorientation of the  $\beta 3$ – $\alpha 3$  loop result in an end-on  $\pi$ -stacking interaction with Phe 86 observed only in the closed, holo form. The side chain of Phe 86 is displaced away from Trp 104 by over 9 Å in the apo, open form. This interaction may stabilize the Trp 140 excited state, increasing its lifetime and decreasing the rate of nonradiative decay in the closed conformation. Phe 86 is not well conserved among cluster A–I SBPs where it is typically substituted with Leu. However, this and the  $\pi$ -stacking interaction with Trp are conserved in the holo forms of *Streptococcus suis* TroA<sup>31</sup> and *Synechocystis* ZnuA<sup>32</sup> crystal structures. This suggests that Trp fluorescence may be sensitive to conformational changes in these proteins as well, although crystallographic evidence suggests a closed apo form for a flexible loop deletion of *Synechocystis* ZnuA<sup>33</sup> and the TroA homologue from *T. pallidum*.<sup>14</sup>

**Thermodynamic Contributions to Binding.** Because of the precipitous transition in signal intensities as the protein approaches saturation, ITC struggles to estimate high-affinity binding constants, but it is a highly accurate means of determining  $\Delta H$ . This is evident from the relative errors on these fitted values in Table 2 as well as the clear underestimation of binding affinity relative to what has been determined by fluorescence assays.<sup>21,22</sup> Nevertheless, what the data unequivocally demonstrate is a large entropic contribution to zinc binding in AztC. To put this into perspective, a  $\Delta S$  of 0 for AztC zinc binding would result in a dissociation constant of 15  $\mu\text{M}$ , approximately 5 orders of magnitude weaker binding affinity than that determined by the MF-2 assay. This is consistent with ITC analysis of other cluster A–I SBPs,<sup>12,31,33,34</sup> where binding to the high-affinity site is insufficiently exothermic or even endothermic and must be driven by a favorable entropic term.

This is generally counterintuitive, especially given the prior discussion of AztC fluorescence where a dynamic equilibrium between open and closed states in the apo form would be expected to have a greater entropy than a purely closed holo form. Desolvation of metal ions upon protein binding may be partly responsible for this increase in entropy, but it is likely that there are also compensatory changes in the dynamics of the holo form, which are not reported by Trp fluorescence. To this end, an analysis of the *B*-factors of holo and apo AztC structures is informative (Figure 5B,C). Unsurprisingly, the previously indicated mobile CTD regions ( $\alpha 7$ – $\beta 6$  loop,  $\alpha 7$ ,  $\alpha 8$ ) and NTD  $\beta 2$ – $\alpha 2$  and  $\beta 3$ – $\alpha 3$  loops exhibit the highest relative *B*-factors in the apo structure. These regions exhibit the greatest conformational change and are stabilized by zinc binding, consistent with a dynamic equilibrium between open and closed states in the apo protein. However, it is interesting to note the increase in relative disorder of NTD helices  $\alpha 2$  and  $\alpha 3$  and the ends of the interdomain helix in the holo structure. These regions are more remote from the metal binding site and may suggest a means of entropic compensation mediating high-affinity zinc binding. Given the positive entropy of binding to other cluster A–I SBPs, this may be a phenomenon of general significance to this protein family.

Taken together, this analysis allows us to construct a more detailed mechanism for zinc binding to AztC. Zinc binding to a relatively open and flexible apo form results in substantial movement in the CTD,  $\beta 2$ – $\alpha 2$ , and  $\beta 3$ – $\alpha 3$  loops, stabilizing the conformations of these regions. This is accompanied by an apparent increase in disorder at the ends of the linker helix and in helices  $\alpha 2$  and  $\alpha 3$ , providing a compensatory increase in entropy and enabling high-affinity zinc binding. Partial unwinding of the C-terminal end of the linker helix upon zinc binding to PsaA may play a similar entropic role,<sup>9</sup> while the decreased mobility of the  $\alpha 2$ – $\beta 2$  loop is reminiscent of zinc binding to AdcA.<sup>19</sup> We also observe partial unwinding and increased flexibility of the  $\alpha 3$  helix upon zinc binding to AztC. It is unknown whether this is conserved in AdcA as there is no crystal structure of the apo form. Thus, AztC exhibits a combination of features observed in other cluster A–I SBPs in addition to some that may be unique, expanding our understanding of the diverse conformational dynamics within this protein family.

## CONCLUSIONS

AztC exhibits dramatic increases of quantum yield and excited-state lifetime upon zinc binding. We propose that the short-lived component in this case represents the open conformation that exists in equilibrium with a smaller component of the closed form in apo AztC. Zinc binding results in conversion entirely to a closed form. The altered fluorescence properties of the closed form are potentially a consequence of a  $\pi$ -stacking interaction between Trp 140 and Phe 86 in holo AztC. In this case, Trp fluorescence can differentiate open and closed states, but this does not preclude the potential existence of other conformations within the closed state. Consistent with this is the observation of a strongly positive entropic component to zinc binding, which may be mediated by increased flexibility of the closed, holo form at regions remote from the metal binding site. Dynamics are likely to be important in recognition of the permease and delivery of zinc, making such studies of particular interest for the development of zinc transfer inhibitors as novel antibiotics. The fluorescence properties of AztC make it a particularly useful probe to

determine how binding of such inhibitors might shift the conformational landscape.

## ASSOCIATED CONTENT

### Accession Codes

AztC: A1B2F3 (Uniprot).

## AUTHOR INFORMATION

### Corresponding Author

Erik T. Yukl – Department of Chemistry and Biochemistry, New Mexico State University, Las Cruces, New Mexico 88003, United States; [orcid.org/0000-0001-6519-6938](https://orcid.org/0000-0001-6519-6938); Phone: 575-646-3176; Email: [etyukl@nmsu.edu](mailto:etyukl@nmsu.edu)

### Author

Fred A. Serrano – Department of Chemistry and Biochemistry, New Mexico State University, Las Cruces, New Mexico 88003, United States

Complete contact information is available at:

<https://pubs.acs.org/10.1021/acsomega.1c06639>

### Author Contributions

E.T.Y. and F.A.S. acquired, analyzed, and interpreted data. E.T.Y. conceived and designed the study and wrote the manuscript.

### Funding

Research reported in this publication was supported by the National Institute of General Medical Science of the National Institutes of Health under award number 1R01GM122819-01.

### Notes

The authors declare no competing financial interest.

## ACKNOWLEDGMENTS

We acknowledge the Department of Chemistry and Biochemistry at New Mexico State University for access to departmental resources and equipment.

## REFERENCES

- (1) Higgins, C. F. ABC transporters: from microorganisms to man. *Annu. Rev. Cell Biol.* **1992**, *8*, 67–113.
- (2) Davidson, A. L.; Dassa, E.; Orelle, C.; Chen, J. Structure, function, and evolution of bacterial ATP-binding cassette systems. *Microbiol. Mol. Biol. Rev.* **2008**, *72*, 317–364 table of contents.
- (3) van der Heide, T.; Poolman, B. ABC transporters: one, two or four extracytoplasmic substrate-binding sites? *EMBO Rep.* **2002**, *3*, 938–943.
- (4) Khare, D.; Oldham, M. L.; Orelle, C.; Davidson, A. L.; Chen, J. Alternating access in maltose transporter mediated by rigid-body rotations. *Mol. Cell* **2009**, *33*, 528–536.
- (5) Bertsson, R. P.-A.; Smits, S. H. J.; Schmitt, L.; Slotboom, D.-J.; Poolman, B. A structural classification of substrate-binding proteins. *FEBS Lett.* **2010**, *584*, 2606–2617. Scheepers, G. H.; Lycklama a Nijeholt, J. A.; Poolman, B. An updated structural classification of substrate-binding proteins. *FEBS Lett.* **2016**, *590*, 4393–4401. From NLM
- (6) Quioco, F. A.; Ledvina, P. S. Atomic structure and specificity of bacterial periplasmic receptors for active transport and chemotaxis: variation of common themes. *Mol. Microbiol.* **1996**, *20*, 17–25.
- (7) Mao, B.; Pear, M. R.; McCammon, J. A.; Quioco, F. A. Hinge-bending in L-arabinose-binding protein. The “Venus’s-flytrap” model. *J. Biol. Chem.* **1982**, *257*, 1131–1133.
- (8) Yatsunyk, L. A.; Easton, J. A.; Kim, L. R.; Sugarbaker, S. A.; Bennett, B.; Breece, R. M.; Vorontsov, I. I.; Tierney, D. L.; Crowder, M. W.; Rosenzweig, A. C. Structure and metal binding properties of

- ZnuA, a periplasmic zinc transporter from *Escherichia coli*. *J. Biol. Inorg. Chem.* **2008**, *13*, 271–288.
- (9) Couñago, R. M.; Ween, M. P.; Begg, S. L.; Bajaj, M.; Zuegg, J.; O'Mara, M. L.; Cooper, M. A.; McEwan, A. G.; Paton, J. C.; Kobe, B.; et al. Imperfect coordination chemistry facilitates metal ion release in the Psa permease. *Nat. Chem. Biol.* **2014**, *10*, 35–41.
- (10) Neupane, D. P.; Avalos, D.; Fullam, S.; Roychowdhury, H.; Yukl, E. T. Mechanisms of zinc binding to the solute-binding protein AztC and transfer from the metallochaperone AztD. *J. Biol. Chem.* **2017**, *292*, 17496–17505.
- (11) Radka, C. D.; Labiuk, S. L.; DeLucas, L. J.; Aller, S. G. Structures of the substrate-binding protein YfeA in apo and zinc-reconstituted holo forms. *Acta Crystallogr., Sect. D: Struct. Biol.* **2019**, *75*, 831–840.
- (12) Abate, F.; Malito, E.; Cozzi, R.; Lo Surdo, P.; Maione, D.; Bottomley, M. J. Apo, Zn<sup>2+</sup>-bound and Mn<sup>2+</sup>-bound structures reveal ligand-binding properties of SitA from the pathogen *Staphylococcus pseudintermedius*. *Biosci. Rep.* **2014**, *34*, No. e00154.
- (13) Sharma, N.; Selvakumar, P.; Bhose, S.; Ghosh, D. K.; Kumar, P.; Sharma, A. K. Crystal structure of a periplasmic solute binding protein in metal-free, intermediate and metal-bound states from *Candidatus Liberibacter asiaticus*. *J. Struct. Biol.* **2015**, *189*, 184–194.
- (14) Lee, Y.-H.; Dorwart, M. R.; Hazlett, K. R. O.; Deka, R. K.; Norgard, M. V.; Radolf, J. D.; Hasemann, C. A. The crystal structure of Zn(II)-free *Treponema pallidum* TroA, a periplasmic metal-binding protein, reveals a closed conformation. *J. Bacteriol.* **2002**, *184*, 2300–2304.
- (15) Tanaka, K. J.; Song, S.; Mason, K.; Pinkett, H. W. Selective substrate uptake: The role of ATP-binding cassette (ABC) importers in pathogenesis. *Biochim. Biophys. Acta Biomembr.* **2018**, *1860*, 868–877.
- Lewis, V. G.; Ween, M. P.; McDevitt, C. A. The role of ATP-binding cassette transporters in bacterial pathogenicity. *Protoplasma* **2012**, *249*, 919–942.
- Klein, J. S.; Lewinson, O. Bacterial ATP-driven transporters of transition metals: physiological roles, mechanisms of action, and roles in bacterial virulence. *Metallomics* **2011**, *3*, 1098–1108.
- Skaar, E. The struggle for metal at the host-pathogen interface. *Faseb. J.* **2018**, *32*, 477.3.
- (16) Deplazes, E.; Begg, S. L.; van Wonderen, J. H.; Campbell, R.; Kobe, B.; Paton, J. C.; MacMillan, F.; McDevitt, C. A.; O'Mara, M. L. Characterizing the conformational dynamics of metal-free PsaA using molecular dynamics simulations and electron paramagnetic resonance spectroscopy. *Biophys. Chem.* **2015**, *207*, 51–60.
- (17) Sridharan, U.; Ragunathan, P.; Spellerberg, B.; Ponnuraj, K. Molecular dynamics simulation of metal free structure of Lmb, a laminin-binding adhesin of *Streptococcus agalactiae*: metal removal and its structural implications. *J. Biomol. Struct. Dyn.* **2019**, *37*, 714–725.
- (18) de Boer, M.; Gouridis, G.; Vietrov, R.; Begg, S. L.; Schuurman-Wolters, G. K.; Husada, F.; Eleftheriadis, N.; Poolman, B.; McDevitt, C. A.; Cordes, T. Conformational and dynamic plasticity in substrate-binding proteins underlies selective transport in ABC importers. *Elife* **2019**, *8*, No. e44652.
- (19) Luo, Z.; Morey, J. R.; Deplazes, E.; Motygullina, A.; Tan, A.; Ganio, K.; Neville, S. L.; Eleftheriadis, N.; Isselstein, M.; Pederick, V. G.; et al. A Trap-Door Mechanism for Zinc Acquisition by *Streptococcus pneumoniae* AdcA. *mBio* **2021**, *12*, No. e01958-20.
- (20) Handali, M.; Roychowdhury, H.; Neupane, D. P.; Yukl, E. T. AztD, a Periplasmic Zinc Metallochaperone to an ATP-binding Cassette (ABC) Transporter System in *Paracoccus denitrificans*. *J. Biol. Chem.* **2015**, *290*, 29984–29992.
- (21) Meni, A.; Yukl, E. T. Structural Features Mediating Zinc Binding and Transfer in the AztABCD Zinc Transporter System. *Biomolecules* **2020**, *10*, 1156.
- (22) Handali, M.; Neupane, D. P.; Roychowdhury, H.; Yukl, E. T. Transcriptional Regulation, Metal Binding Properties and Structure of Pden1597, an Unusual Zinc Transport Protein from *Paracoccus denitrificans*. *J. Biol. Chem.* **2015**, *290*, 11878–11889.
- (23) Wang, Y.; Graichen, M. E.; Liu, A.; Pearson, A. R.; Wilmot, C. M.; Davidson, V. L. MauG, a novel di-heme protein required for tryptophan tryptophylquinone biogenesis. *Biochemistry* **2003**, *42*, 7318–7325.
- (24) Edelhoch, H. Spectroscopic determination of tryptophan and tyrosine in proteins. *Biochemistry* **1967**, *6*, 1948–1954.
- (25) Chen, R. F. Fluorescence Quantum Yields of Tryptophan and Tyrosine. *Anal. Lett.* **1967**, *1*, 35–42.
- (26) Eftink, M. R. *Techniques for Studying Protein Structure*; John Wiley & Sons, Inc., 1991.
- (27) Szabo, A. G.; Stepanik, T. M.; Wayner, D. M.; Young, N. M. Conformational heterogeneity of the copper binding site in azurin. A time-resolved fluorescence study. *Biophys. J.* **1983**, *41*, 233–244.
- (28) Grinvald, A.; Schlessinger, J.; Pecht, I.; Steinberg, I. Z. Homogeneity and variability in the structure of azurin molecules studied by fluorescence decay and circular polarization. *Biochemistry* **1975**, *14*, 1921–1929.
- (29) Petrich, J. W.; Longworth, J. W.; Fleming, G. R. Internal motion and electron transfer in proteins: a picosecond fluorescence study of three homologous azurins. *Biochemistry* **1987**, *26*, 2711–2722.
- Ugurbil, K.; Bersohn, R. Nuclear magnetic resonance study of exchangeable and nonexchangeable protons in azurin from *Pseudomonas aeruginosa*. *Biochemistry* **1977**, *16*, 3016–3023.
- (30) Munro, I.; Pecht, I.; Stryer, L. Subnanosecond motions of tryptophan residues in proteins. *Proc. Natl. Acad. Sci. U.S.A.* **1979**, *76*, 56–60.
- (31) Zheng, B.; Zhang, Q.; Gao, J.; Han, H.; Li, M.; Zhang, J.; Qi, J.; Yan, J.; Gao, G. F. Insight into the interaction of metal ions with TroA from *Streptococcus suis*. *PLoS One* **2011**, *6*, No. e19510.
- (32) Banerjee, S.; Wei, B.; Bhattacharyya-Pakrasi, M.; Pakrasi, H. B.; Smith, T. J. Structural determinants of metal specificity in the zinc transport protein ZnuA from *Synechocystis* 6803. *J. Mol. Biol.* **2003**, *333*, 1061–1069.
- (33) Wei, B.; Randich, A. M.; Bhattacharyya-Pakrasi, M.; Pakrasi, H. B.; Smith, T. J. Possible regulatory role for the histidine-rich loop in the zinc transport protein, ZnuA. *Biochemistry* **2007**, *46*, 8734–8743.
- (34) Desrosiers, D. C.; Sun, Y. C.; Zaidi, A. A.; Eggers, C. H.; Cox, D. L.; Radolf, J. D. The general transition metal (Tro) and Zn<sup>2+</sup> (Znu) transporters in *Treponema pallidum*: analysis of metal specificities and expression profiles. *Mol. Microbiol.* **2007**, *65*, 137–152.
- Neupane, D. P.; Kumar, S.; Yukl, E. T. Two ABC Transporters and a Periplasmic Metallochaperone Participate in Zinc Acquisition in *Paracoccus denitrificans*. *Biochemistry* **2018**, *58*, 126.